Onset of Irreversible Reactions in Overcharging Lithium-Ion Cells: an Experimental and Modeling Approach

Elisa Irujo
Dept. of Electrical, Electronic and Communications Engineering
Public University of Navarre (UPNA)
Pamplona, Spain
elisa.irujo@unavarra.es

Alberto Berrueta
Institute of Smart Cities,
Dept. of Electrical, Electronic and Communications Engineering
Public University of Navarre (UPNA)
Pamplona, Spain
alberto.berrueta@unavarra.es

Iñaki Lalinde
Institute of Smart Cities,
Dept. of Electrical, Electronic and Communications Engineering
Public University of Navarre (UPNA)
Pamplona, Spain
inaki.lalinde@unavarra.es

Joseba Arza
Ingeteam R&D Europe,
Zamudio, Spain
joseba.arza@ingeteam.com

Pablo Sanchis
Institute of Smart Cities,
Dept. of Electrical, Electronic and Communications Engineering
Public University of Navarre (UPNA)
Pamplona, Spain
pablo.sanchis@unavarra.es

Alfredo Ursúa
Institute of Smart Cities,
Dept. of Electrical, Electronic and Communications Engineering
Public University of Navarre (UPNA)
alfredo.ursua@unavarra.es

***Abstract*—Lithium-ion batteries are energy storage systems used in an increasing number of applications. Due to their flammable materials, their use entails risks of fire and explosion. The study of the abuse operation of these batteries before reaching the thermal runaway is a relevant research topic to prevent safety issues. There are various studies in the bibliography providing exhaustive thermal studies of the safe operating area, as well as concerning the thermal runaway. However, the onset irreversible reactions, that take place at a SOC around 110%, have not been properly analyzed. We present in this contribution an experimental study of this onset reaction measured in pouch Li-ion cells under various conditions of charge current and temperature. We also propose a lumped-parameter thermal model for the cell, which allows a detailed characterization of this exothermic reaction. The results achieved in this contributions can be a key tool to prevent overcharge accidents that may arise due to malfunctioning of the battery charger or battery management system.**

***Index Terms*—Lithium-Ion Battery, Overcharge, Thermal runaway**

I. Introduction

On the way to descarbonization and energy independence, energy storage systems play a key role in emerging applications such as electric vehicles and the grid integration of renewable energy. Particularly, lithium-ion batteries (LIBs) is one of the potential energy storage solutions due to its high energy and power density, long life and low self-discharge [1].

However, Li-ion batteries may entail safety issues due to the properties of their materials. The applications of LIBs are limited by temperature and voltage operating ranges, which delineate the so-called Safe Operating Area (SOA) [2]. To assure proper voltage and temperature conditions, the battery state is monitored and controlled by the battery management system (BMS) which normally integrates an active thermal management system (BTMS) [3]. Nevertheless, a malfunctioning of the BMS or a construction problem can lead to exceeding the limits and bring batteries to less efficient performance. Moreover, outside the SOA, irreversible reactions take place, reducing the available active material and, consequently, the battery capacity [4]. A particular side reaction known as lithium plating may start due to a deficient lithium intercalation in the anode mainly due to fast charges at low temperature. This may lead to the formation of lithium dendrites, which have the potential of punching the cell separator, thereby short-circuiting the cell by means of an internal short circuit (ISC).

When the operating temperature exceeds the maximum limit set by the manufacturer, additional degradation processes are set. If this temperature keeps increasing, self-maintained exothermic reactions are triggered, leading to a thermal runaway (TR) and the subsequent battery self-destruction [5]. TR events are mainly due to abuse conditions such as overcharge, over temperature and impact. Overcharge situation are the most hazardous events, since the battery stores a greater

This work is part of the projects PID2019-111262RB-I00, funded by MCIN/AEI/10.13039/501100011033/, TED2021-132457B-I00, funded by MCIN/AEI/10.13039/501100011033/ and by the European Union NextGenerationEU/PRTR, STARDUST (774094), funded by European Union's Horizon 2020 research and innovation programme, HYBPLANT (0011-1411-2022-000039), funded by Government of Navarre, and has also been supported by MCIN/AEI/10.13039/501100011033/ and by European Social Fund under a PhD scholarship (grant PRE2020-095314).

amount of energy, which is released in the TR [3]. Thus, characterizing the overcharge behavior is essential to allow a proper evaluation of preventive or predictive methods to avoid accidents in Li-ion batteries.

A number of research works concerning the overcharge operation of Li-ion batteries have been recently published in the scientific bibliography. Zhu et al. tested LIBs at various current rates at room temperature, and characterized four stages in the overcharge process [6]. Wang et al. studied the behavior of the LIBS from the beginning of the overcharge to the TR in four cells with different cathode materials and proposed a safety assessment score system to address the chance of a TR [7]. These two studies keep track of cell temperature, voltage and internal resistance. Other authors [8] include in their studies capacity measurements at different overcharge SOCs, identifying 122% as the beginning of an accelerated degradation. A detailed characterization of the TR as a function of the overcharge level was published by Mao et al. [9]. LIBs are analyzed at six overcharge SOCs from 100 to 150% and their TRs are compared. A modification of the electrode materials at 150% SOC is identified in this study the lead to more severe TR events in this overcharging region. Finally, TR models are published to complement experimental studies and to allow a more detailed analysis of the involved phenomena. This modeling approach provides detailed conclusions with a lower amount of experimental work, thereby reducing the required equipment and materials to expose the cell to various conditions. An electro-thermal coupled model is proposed by Ren et al. to simulate the behavior of LIBs under overcharged conditions till TR [10], while Lalinde et al. built a model based on chemical kinetics, which meant a relevant reduction in the number of parameters and required information concerning the chemical composition of the studied LIB to carry out the TR analysis [11].

We present in this contribution a detailed experimental analysis of the overcharge region of Li-ion cells in order to characterize the triggering of accelerated degradation mechanisms in this abuse region. With this aim, overcharge experiments carried out with six pouch Li-ion cells under various temperature and C-rate conditions are presented. The cells are charged up to $SOC = 150\%$, measuring voltage, temperature and internal resistance. The purpose of this work is to contribute to the understanding of the overcharge behavior of LIBs, characterizing early degradation mechanisms. With this aim, a thermal lumped model is proposed in order to find the required parameters to model each process that contributes to the cell temperature rise. The presented experiments show an exothermic reaction taking place for $110\% \leq SOC \leq 115\%$. To the best of our knowledge, this is the second time at which this phenomena has been registered and published. Ye et al. registered a similar effect during adiabatic overcharge experiments [12]. The novelty of our contribution is the characterization of this phenomenon in a new Li-ion battery technology and by means of non-adiabatic experimental procedure.

The content of this contribution is organized as follows. Section II provides a description of the tested battery, the overcharge experimental procedure and the test bench assembly. Section III presents the energy balance considered in this study and the estimation of the parameters needed for the calculation of the heat contributors. These expressions are employed in Section IV, along with the experimental results, to characterize the first reactions that take place in the overcharge area. Finally, the main conclusions of the study are drawn in Section V.

II. Experimental setup

A. Battery description

The overcharge experiments presented in this contribution are conducted with six pouch Li-ion cells, with a nominal capacity $C_n = 3.6$ Ah. Specifically, the cell model is SLPB8643128H5, manufactured by Kokam Co., Ltd. The cell nominal voltage is 3.7 V, being the operating voltage range 2.7 – 4.2 V. The 96,3 g cell has dimensions of 129 mm height, 43 mm width and 8.8 mm thick.

The cathode material is a mixture of NMC and LCO, while the anode is made of a carbon/graphite composition. The electrolyte consists in a solution of lithium hexafluorophosphate ($LiPF_6$) in a mixture of two organic solvents: ethylene carbonate (EC) and ethyl methyl carbonate (EMC).

B. Overcharge experiments

The following experimental procedure is established in order to guarantee accurate measurements and comparability among different results. The first parameter to be measured is the capacity each cell. It is measured under controlled temperature conditions at 25ºC, by means of three charge–discharge cycles, with CC-CV charges at C/3 (cut off current of C/20), and CC discharges at C/3. The voltage limits are 4.2 V and 2.7 V, as stated by the manufacturer. The discharged capacity in the third cycle is considered the actual capacity of the cell (C_a), which may be different from the nominal capacity. After this measurement, at $SOC = 0\%$, the cell temperature is set to the conditions required in each experiment.

Six overcharging experiments are conducted at different temperature and C-rate combinations by CC-charging the cell from $SOC = 0\%$ to $SOC = 150\%$. On the one hand, the first four experiments are conducted at an ambient temperature of 25ºC, charging the cells different C-rates (1, 0.75, 0.5 and 0.25). They are *Test 1*, *Test 2*, *Test 3* and *Test 4*, respectively. On the other hand, the last two experiments are carried out with a C-rate of 0.75, with ambient temperatures of 50ºC and 75ºC. They are *Test 5* and *Test 6*, respectively.

The temperature, voltage and current are measured during the overcharge experiments. Moreover, the experiments include 10-second pauses every 10 minutes in order to measure the internal DC resistance, R_{DC}. At these current interruptions, R_{DC} can be computed as follows:

$$R_{DC} = \frac{\Delta V}{\Delta I}, \tag{1}$$

where ΔV is the voltage variation and ΔI the current variation at each current interruption of 10 seconds.

Fig. 1. Configuration of the test bench: power source and current and voltage data logger on the left, and a cell inside a resistant stainless-steel oven with temperature data logger on the right.

C. Test bench

The experiments presented in this contribution are performed in the Laboratory for Energy Storage and Microgrids of the Public University of Navarre (UPNA), in the test bench shown in Fig. 1. Capacity measurements are conducted in an Ineletec INECC-30/150 thermal chamber at a controlled temperature of 25°C, whereas the overcharge experiments are carried out inside the 80 L resistant stainless steel oven shown in Fig. 1, which reaches a maximum temperature of 220°C.

The charging and discharging processes are done by means of a Xantrex xdc 300–20, a programmable digital DC power source. Voltage and current measurements are recorded through a Yokogawa WT3000 data logger. To measure the cell temperature, 5 type K thermocouples are attached at various points of the cell, as shown in Fig. 2 (a). Given the temperature gradients of the cell, the average of the five measurements is considered to be the cell temperature (T_{cell}). Moreover, the average between 2 additional thermocouples is used to measure the ambient temperature inside the oven (T_{amb}). The cold-junction compensated thermocouple-to-digital converter MAX31855 is used as analog-to-digital converter for temperature measurements. This device offers an accuracy of ±2°C for temperatures between –200°C and 700°C. Finally, a Raspberry Pi 3B+ with a sampling frequency of 15 Hz is used as data logger for temperature measurements, as shown in Fig. 2 (b).

III. Analysis of Thermal Phenomena

A. Energy balance

During the charging process, the cell experiences an increase in temperature, given that the heat generated by physico-chemical processes ($\dot{Q}_{gen}$) is larger than the heat dissipated with to the surroundings ($\dot{Q}_{dis}$). This leads to an increased thermal energy accumulated in the cell ($\dot{Q}_{cell}$), which can be expressed through the following energy balance:

$$mC_p \frac{dT_{cell}}{dt} = \dot{Q}_{cell} = \dot{Q}_{gen} - \dot{Q}_{dis}, \tag{2}$$

(a) (b)

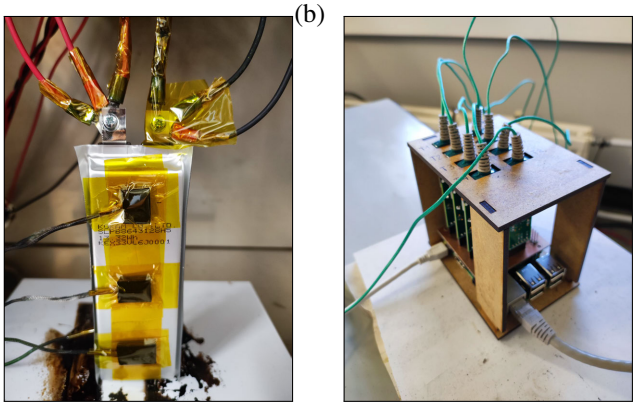

Fig. 2. Temperature measurement: a) sensor positions on the cell, and b) temperature data logger.

where m [g] is the cell mass and $C_p \left[\frac{J}{gK}\right]$ is the heat capacity. The heat generated during the overcharge experiments is due to side reactions ($\dot{Q}_{side}$) and due to the Joule effect ($\dot{Q}_{ohm}$). Thus, the heat generated is expressed as:

$$\dot{Q}_{gen} = \dot{Q}_{side} + \dot{Q}_{ohm}. \tag{3}$$

In this equation, the ohmic heat can be calculated as follows:

$$\dot{Q}_{ohm} = I^2 R_{DC}, \tag{4}$$

where I is the battery charging current. This ohmic contribution dominates heat generation processes during the safe operating area, whereas the side reactions acquire a larger relevance at $SOC > 100\%$.

A fraction of this generated heat is exchanged with the surrounding environment by means of convection and radiation. The convective heat transfer rate follows Newton's law:

$$\dot{Q}_{conv} = h_{conv} A (T_{cell} - T_{amb}), \tag{5}$$

where $h_{conv} \left[\frac{W}{m^2 K^4}\right]$ is the convective transfer coefficient, and $A \left[m^2\right]$ is the surface area. On the other hand, the radiative heat transfer rate is expressed through the Stefan-Botlzman law:

$$\dot{Q}_{rad} = h_{rad} A (T_{cell} - T_{amb}), \tag{6}$$

where $h_{rad} = \varepsilon\sigma(T_{cell} + T_{amb})({T_{cell}}^2 + {T_{amb}}^2)$, being ε the emissivity coefficient, and σ the Stefan-Boltzmann constant ($5.67 \cdot 10^{-8} \frac{W}{m^2 K^4}$). The addition of convective and radiative heat transfer terms provides the total heat dissipation rate:

$$\dot{Q}_{dis} = \dot{Q}_{conv} + \dot{Q}_{rad} = (h_{conv} + h_{rad}) A (T_{cell} - T_{amb}) \tag{7}$$

B. Thermal model for the Li-ion cell

A lumped model of the energy balance described in Subsection III-A is used to analyze the thermal behavior of the cell. To build the equivalent electric circuit, certain parameters are required, as shown in Fig. 3. A capacitor models the heat accumulation, a resistor mimics the heat transfer phenomena, a current source represents the heat generation and the voltage source sets the ambient temperature.

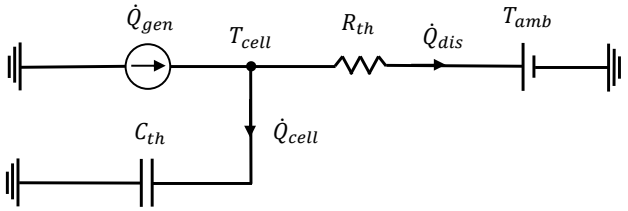

Fig. 3. Thermal model for the Li-ion cell.

Firstly, the thermal resistance (R_{th}) is defined as:

$$R_{th} = \frac{1}{(h_{conv} + h_{rad})A}. \tag{8}$$

The calculation of R_{th} for the cell studied in this contribution is based on the steady-state data measured during constant-heating experiments in the safe operating area, by means of the following expression:

$$R_{th} = \left.\frac{T_{cell} - T_{amb}}{\dot{Q}_{gen}}\right|_{ss}, \tag{9}$$

where the $_{ss}$ subscript stands for steady state. R_{th} is calculated for each experiment using as steady state period for T_{cell} and T_{amb} the last 5 minutes before reaching $SOC = 100\%$. The internal resistance (R_{DC}) is determined by means of (1). Given that Joule heating is the mayor contributor of heat generation in normal operating range, only this term is considered for the calculation of $\dot{Q}_{gen}$:

$$\dot{Q}_{gen}(SOC < 100\%) \approx \dot{Q}_{ohm} = I^2 R_{DC} \tag{10}$$

The data measured and used for this calculation is compiled into Table I. The average value $R_{th} = 18$ºC/W matches with previous studies with similar cells published in the bibliography [13].

On the other hand, the heat capacity (C_{th}) can be calculated as follows:

$$C_{th} = mC_p, \tag{11}$$

where C_p value is extracted from published studies. Liu et al. used an accelerated rate calorimeter to measure the specific thermal capacity of a cell with similar characteristics to the one used in this contribution, obtaining a value of $C_p = 1101 \frac{J}{kgK}$ [14], which is the value selected for our model.

TABLE I
EXPERIMENTAL RESULTS USED TO COMPUTE R_{th}.

Test ID	$T^{ss}_{cell}\,[^\circ C]$	$T^{ss}_{amb}\,[^\circ C]$	$R^{ss}_{DC}\,[m\Omega]$	$R_{th}\left[\frac{^\circ C}{W}\right]$
1	29.22	22.97	33.15	14
2	26.96	21.18	33.33	23
3	25.57	24.75	13.88	17
4	23.49	22.93	24.85	25
5	53.87	49.77	45.57	12
6	76.19	74.94	8.84	19

IV. RESULTS AND DISCUSSION

A. Experimental results

The variables measured during the constant-current overcharge experiments are compiled in this subsection. Specifically, the voltages are represented by means of the red color range, temperatures with the blue color range and internal resistances with the green color range. On the one hand, Fig. 4 (a) illustrates the results of the experiments at a temperature $T_{amb} = 25 \pm 3$ºC and different C-rates (Test 1, 2, 3 and 4). On the other hand, Fig. 4 (b) shows the experiments performed with $I = 0.75$ C and different ambient temperatures (Test 2, 5 and 6). Test 2, whose conditions are $T_{amb} = 25$ ºC and $I = 0.75$ C, is the intersection between both series of experiments. The SOC shown in the horizontal axis of both figures is calculated as follows:

$$SOC = \frac{1}{C_a}\int I(t)dt. \tag{12}$$

The cell temperatures measured in all the experiments show a similar trend during safe operating area (SOA). T_{cell} increases until the heat generated by Joule effect equals the dissipated heat and the temperature remains constant. This leads the cell to a thermal steady-state operation, as anticipated for the calculation of R_{th} in (9). The SOC range at which the cell is charged at a thermal steady state is from $SOC = 80\%$ to $SOC = 100\%$. It should be noted from Fig. 4 (a) that the higher the current, the higher the temperature reached. This rising temperature is one of the reasons for the reduction of R_{DC} at the beginning of the experiments.

After the SOA, when the cell enters the overcharge area, the voltage continues rising as it does in the final part of the SOA, and the temperature remains stable at steady-state value for $100 \leq SOC \leq 110\%$. This constant temperature indicates that the cells behaves in this region as in the SOA. However, a sensible temperature rise begins at $SOC = 110\%$, along with a reduction of the voltage slope matching with the starting of a slight swelling visible during the experiments. Therefore, this SOC value is associated with the beginning of exothermal reactions that release gases. The six experiments presented in this contribution show a similar heat up and a similar cooling process before continuing to increase in temperature, in line with the previous published results mentioned in the introduction [12]. The larger is the current or ambient temperature, the faster the temperature rises.

After this effect, for $SOC \geq 115\%$, R_{DC} has a sensible rise, starting from values of $R_{DC} \approx 20$ mΩ and reaching values as high as $R_{DC} \approx 200$ mΩ at $SOC = 150\%$. This increase in the internal resistance is attributed to the fast degradation of cell materials and to the gas generation inside the cell. Note that in Test 6, with $T_{amb} = 75$ºC, the cell voltage suffers a sharp increase due to the chemical reactions that take place at this combination of SOC and temperature and, a TR could probably have occurred if the overcharge had continued above 150%.

The exothermic reaction detected at $110 \leq SOC \leq 115\%$ indicates the beginning of accelerated and irreversible cell

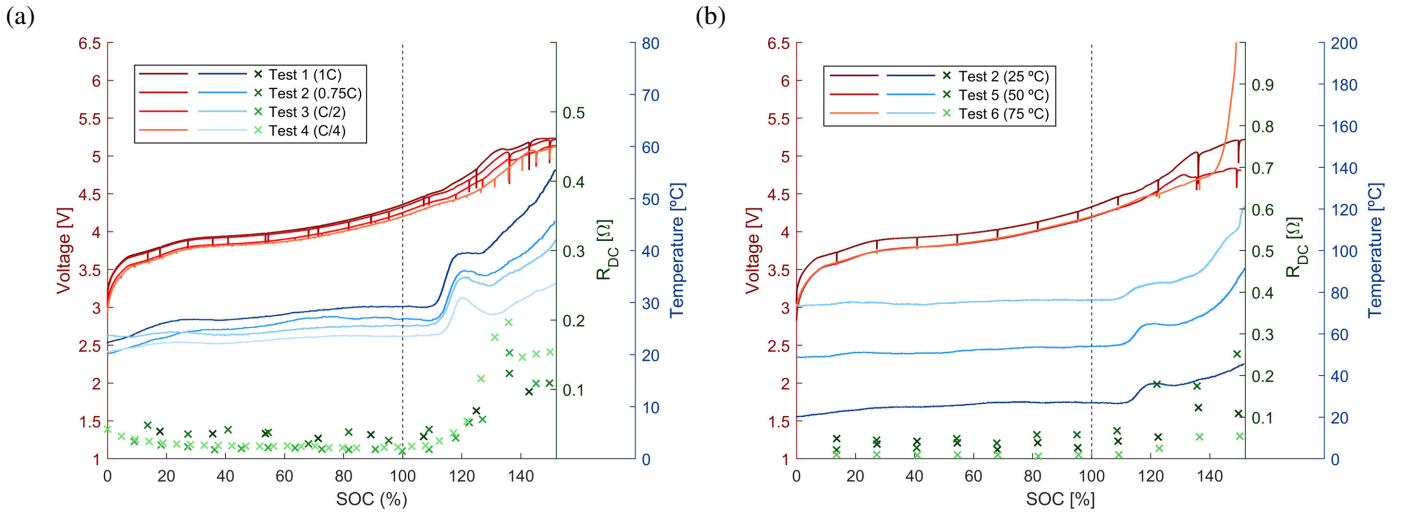

Fig. 4. Experimental measurements for overcharging experiments: voltage in red, solid line (left axis), temperature in blue, solid line and internal resistance in green markers (right axis). a) Different C-rates at 25ºC, and b) different ambient temperatures at 0.75C.

degradation, which should be avoided for a proper operation of a LIB. A detailed characterization of this undesired reaction is shown in Table II. The starting point for this reaction is considered when all thermocouples measure a heating rate higher than 0. The parameters SOC_{start}, T_{cell}^{start} and V_{start} shown in the table are measured at this time. Similarly, the end of this phenomenon is considered when all thermocouples capture a temperature rate lower than 0. SOC_{end} is measured at this time. ΔT, is calculated as $\Delta T = T_{cell}^{end} - T_{cell}^{start}$, where T_{cell}^{end} is the temperature at SOC_{end}. Finally, the last column, E, is the energy associated to the exothermic reaction, calculated from $\dot{Q}_{side}$ by means of the following expression:

$$E = \int_{SOC_{start}}^{SOC_{end}} \dot{Q}_{side} dt. \tag{13}$$

B. Analysis of the onset degradation reaction

A break-down of the heat generation measured during this reaction, based on the model proposed in Subsection III-B, is presented for a better understanding of the underlying processes. Based on the experimental results, $\dot{Q}_{dis}$ is calculated by means of (7) and (8), and $\dot{Q}_{cell}$ is obtained as expressed in (2). Taking the internal resistance and current of each experiment $\dot{Q}_{ohm}$ is calculated by means of (3). Finally, $\dot{Q}_{side}$ can be obtained after solving (2) and (4).

Fig. 5 displays the four heat contributors considered in this study. The results of Test 1 are selected as a representative example. Starting at $SOC = 90\%$, it can be observed the heating of the cell due solely to the ohmic heat, since cell temperature reaches steady state being $Q_{ohm} \approx Q_{dis}$, as assumed above. At $107\% \leq SOC \leq 122\%$, a sudden and abrupt heat generation due to the onset degradation reaction can be appreciated. As Q_{ohm} increases only slightly, this enormous amount of heat generated is attributed to Q_{side}. At $SOC > 130\%$, further irreversible reactions drive the cell to advanced degradation states. As the cell temperature

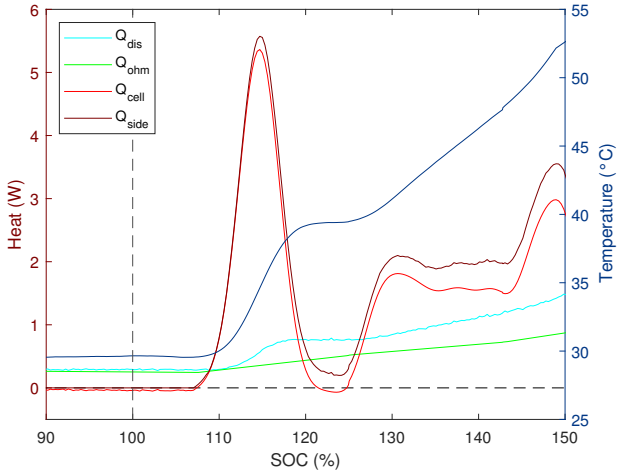

Fig. 5. Deployment of heat contributors in Test 1.

increases, the dissipated heat is also augmented, due to the larger difference between T_{cell} and T_{amb}.

Fig. 6 shows a closer analysis of the heat generated exclusively due to side reactions around onset degradation phenomenon extracted from the six experiments. Note that the maximum heat value reached depends on the overcharging current. However, the energy delivered in all the experiments is similar. The last column of Table II presents the energy released in this reaction, providing an average value of 1010,1 J and a range of $\pm 10\%$ in all the experiments.

V. Conclusions

This paper presents an experimental overcharge characterization of a 3.6 Ah pouch Li-ion cell. To do so, six cells are subjected to overcharging experiments up to $SOC = 150\%$ under different current and temperature conditions, while

TABLE II
CHARACTERISTIC PARAMETERS FOR THE ONSET DEGRADATION MECHANISM IN THE SIX EXPERIMENTS

Test ID	C-rate	$T_{amb}\,[^\circ C]$	$SOC_{start}\,[\%]$	$T_{cell}^{start}\,[^\circ C]$	$V_{start}\,[V]$	$SOC_{end}\,[\%]$	$\Delta T\,[^\circ C]$	$E\,[J]$
1	1	25	109.3	29.25	4.46	121.4	10.25	1108.2
2	0.75	25	109.9	26.75	4.47	122.5	9.25	1109.6
3	0.5	25	112.5	26.75	4.41	122.3	7.75	1048.0
4	0.25	25	112.9	24.00	4.37	120.2	6.75	927.6
2	0.75	25	109.9	26.75	4.47	122.5	9.25	1109.6
5	0.75	50	109.6	54.75	4.30	122.9	9.75	882.5
6	0.75	75	108.0	76.75	4.30	123.3	7.75	984.6

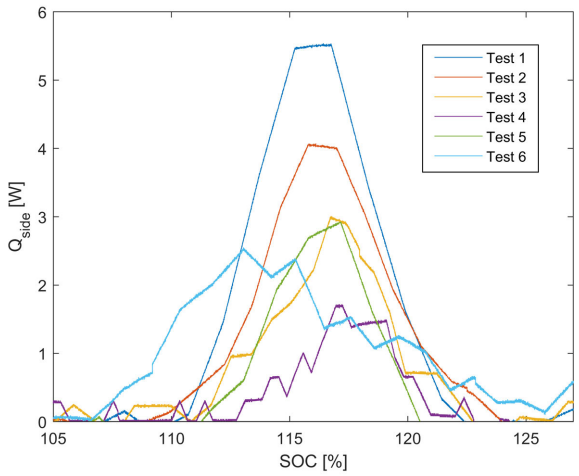

Fig. 6. Heat generation by side reaction.

monitoring voltage, temperature and internal resistance. This characterization contributes to the understanding of Li-ion cell behavior under overcharge conditions. Overcharge accidents due to safety failures still take place and the characterization of this area is crucial to detect the beginning of this kind of events, thereby allowing the design of devices or mechanisms to prevent it.

In addition to the experimental characterization, this contribution proposes a simplified thermal lumped model that allows a comprehensive analysis of these experimental measurements. Using this model, the onset mechanism that drives the cell to irreversible exothermal degradation reactions is identified. The proposed tool allows the detailed characterization of the reaction that takes place approximately from $SOC = 110\%$ to $SOC = 122\%$, releasing an energy of 1010 J $\pm 10\%$. After discussing the results, it can be concluded that there is an onset SOC in this kind of Li-ion cells at which this phenomenon occurs and the released energy is independent of temperature and current conditions.

Thus, this reaction means the beginning of the cell accelerated degradation and provides a starting point for designing preventive mechanisms to avoid the thermal runaway. This reaction is attributed to the decomposition of the weakest material that builds the cell. This triggering phenomena has not yet been deeply analyzed from the materials point of view and, therefore, its reasons have not been clearly defined. The results presented in this contribution can be used as the basis for deeper analysis about this onset mechanism. The relevance of this study lies on the identification of this warning mechanism to avoid overcharging accidents.

REFERENCES

[1] L. Lu, X. Han, J. Li, J. Hua, and M. Ouyang, "A review on the key issues for lithium-ion battery management in electric vehicles," *Journal of Power Sources*, vol. 226, pp. 272–288, 2013.

[2] J. Duan, X. Tang, H. Dai, Y. Yang, W. Wu, X. Wei, and Y. Huang, "Building safe lithium-ion batteries for electric vehicles: A review," *Electrochemical Energy Reviews*, vol. 3, pp. 1–42, 2019.

[3] I. Lalinde, A. Berrueta, J. J. Valera, J. Arza, P. Sanchis, and A. Ursúa, "Perspective chapter: Thermal runaway in lithium-ion batteries," in *Lithium-Ion Batteries - Recent Advanced and Emerging Topics*, D. G. Lamblin, Ed. Rijeka: IntechOpen, 2022, ch. 3.

[4] W. Li, S. Rao, Y. Xiao, Z. Gao, Y. Chen, H. Wang, and M. Ouyang, "Fire boundaries of lithium-ion cell eruption gases caused by thermal runaway," *iScience*, vol. 24, no. 5, p. 102401, 2021.

[5] X. Feng, M. Ouyang, X. Liu, L. Lu, Y. Xia, and X. He, "Thermal runaway mechanism of lithium ion battery for electric vehicles: A review," *Energy Storage Materials*, vol. 10, pp. 246–267, 2018.

[6] X. Zhu, Z. Wang, Y. Wang, H. Wang, C. Wang, L. Tong, and M. Yi, "Overcharge investigation of large format lithium-ion pouch cells with li(ni0.6co0.2mn0.2)o2 cathode for electric vehicles: Thermal runaway features and safety management method," *Energy*, vol. 169, pp. 868–880, 2019.

[7] Z. Wang, J. Yuan, X. Zhu, H. Wang, L. Huang, Y. Wang, and S. Xu, "Overcharge-to-thermal-runaway behavior and safety assessment of commercial lithium-ion cells with different cathode materials: A comparison study," *Journal of Energy Chemistry*, vol. 55, pp. 484–498, 2021.

[8] M. Ouyang, D. Ren, L. Lu, J. Li, X. Feng, X. Han, and G. Liu, "Overcharge-induced capacity fading analysis for large format lithium-ion batteries with liyni1/3co1/3mn1/3o2+liymn2o4 composite cathode," *Journal of Power Sources*, vol. 279, pp. 626–635, 2015.

[9] N. Mao, Z.-R. Wang, Y.-H. Chung, and C.-M. Shu, "Overcharge cycling effect on the thermal behavior, structure, and material of lithium-ion batteries," *Applied Thermal Engineering*, vol. 163, p. 114147, 2019.

[10] D. Ren, X. Feng, L. Lu, M. Ouyang, S. Zheng, J. Li, and X. He, "An electrochemical-thermal coupled overcharge-to-thermal-runaway model for lithium ion battery," *Journal of Power Sources*, vol. 364, pp. 328–340, 2017.

[11] I. Lalinde, A. Berrueta, P. Sanchis, and A. Ursúa, "Applied method to model the thermal runaway of lithium-ion batteries," pp. 1–6, 2021.

[12] J. Ye, H. Chen, Q. Wang, P. Huang, J. Sun, and S. Lo, "Thermal behavior and failure mechanism of lithium ion cells during overcharge under adiabatic conditions," *Applied Energy*, vol. 182, pp. 464–474, 2016.

[13] E. Paccha-Herrera, W. R. Calderón-Muñoz, M. Orchard, F. Jaramillo, and K. Medjaher, "Thermal modeling approaches for a licoo2 lithium-ion battery—a comparative study with experimental validation," *Batteries*, vol. 6, no. 3, 2020.

[14] J. Liu, Z. Wang, J. Bai, T. Gao, and N. Mao, "Heat generation and thermal runaway mechanisms induced by overcharging of aged lithium-ion battery," *Applied Thermal Engineering*, vol. 212, p. 118565, 2022.